Article

Myocyte Enhancer Factor 2A (MEF2A) Defines Oxytocin-Induced Morphological Effects and Regulates Mitochondrial Function in Neurons

Magdalena Meyer[1], Kerstin Kuffner[2], Julia Winter[1], Inga D. Neumann[1], Christian H. Wetzel[2] and Benjamin Jurek [1,*]

[1]   1 Department of Behavioral and Molecular Neurobiology, and [2] Department of Psychiatry and Psychotherapy, University of Regensburg, Regensburg, Germany;

[*]   Correspondence: Benjamin.jurek@ur.de;

  Abstract:

The neuropeptide oxytocin (OT) is a well-described modulator of socio-emotional traits, such as anxiety, stress, social behavior, and pair-bonding, however, when dysregulated, it is associated with adverse psychiatric traits, like various aspects of autism spectrum disorder (ASD). In this study, we identify the transcription factor MEF2A as the common link between OT and cellular changes symptomatic for ASD, encompassing neuronal morphology, connectivity, and mitochondrial function. We provide evidence for MEF2A as the decisive factor defining the cellular response to OT: while OT induces neurite retraction in MEF2A expressing neurons, OT causes neurite outgrowth in absence of MEF2A. A CRISPR-Cas-mediated knockout of MEF2A and retransfection of an active version or permanently inactive mutant, respectively, validated our findings. We also identified the phosphatase calcineurin as the main upstream regulator of OT-induced MEF2A signaling. Further, MEF2A signaling dampens mitochondrial functioning in neurons, as MEF2A knockout cells show increased maximal cellular respiration, spare respiratory capacity, and total cellular ATP.

In summary, we reveal a central role for OT-induced MEF2A activity as major regulator of cellular morphology as well as neuronal connectivity and mitochondrial functioning, with broad implications for a potential treatment of disorders based on morphological alterations or mitochondrial dysfunction.

Keywords: oxytocin, morphology, neurite outgrowth, neurite retraction, autism, MEF2A, CRISPR-Cas, hyperconnectivity

1. Introduction

Oxytocin (OT) is a neuropeptide profoundly implicated in the regulation of various socio-emotional behaviors and physiological responses (Jurek and Neumann, 2018). Dysregulated plasma or salivary levels of OT have been associated with symptoms of autism spectrum disorder (ASD) (Alaerts et al., 2019; Parker et al., 2014), depression (Yuen et al., 2014), and anxiety (Carson et al., 2015), and its intranasal application has been described to relieve some of those symptoms (Meyer-Lindenberg et al., 2011). As a multifactorial disorder, ASD has been associated with neuronal, morphological and mitochondrial dysfunctions (Bringas et al., 2013; Falougy et al., 2019; Garcia-Cabezas et al., 2018; Maes et al., 2019; Young et al., 2016). One common factor between ASD, its underlying disturbed cellular functions and the oxytocinergic system, is the transcription factor myocyte enhancer factor (MEF) 2. In this study, we provide evidence for the role of MEF2 as the central node in the regulation of those conditions.

One major parameter in ASD patients is an alteration of the neuronal connectivity. Autistic patients show hyperconnectivity between amygdala and hippocampus, which is negatively correlated with peripheral OT levels, and can even be further decreased by intranasal application of OT (Alaerts et al., 2019). Furthermore, neurons generated from iPSCs of ASD patients have more complex and longer neurites, causing increased synapse number and a state of hyperconnectivity (Tang et al., 2014; Zaslavsky et al., 2019). MEF2 is one factor being responsible for the regulation of excitatory synapse number (Flavell et al., 2006; Morrow et al., 2008; Shalizi et al., 2006), and we have recently provided evidence for its activation by OT receptor-coupled signaling pathways (Meyer et al., 2018). The activation of Gq protein-coupled OT receptors lead to an increase in intracellular calcium from either intracellular stores (Sanborn, 2007), through cation channels such as TrpV2/4 (van den Burg et al., 2015; Ying et al., 2015) or L-type voltage-gated calcium channels (Zatkova et al., 2018). Upon OT-induced calcium influx, the phosphatase calcineurin (CaN, or protein phosphatase 2B; PP2B) is activated by binding calmodulin (Pont et al., 2012). Active CaN acts on the one hand as direct phosphatase of cytoskeletal proteins and influences the stability and interaction

of microtubule and actin filaments (Descazeaud et al., 2012; Lautermilch and Spitzer, 2000; Xiong et al., 2018). On the other hand, it dephosphorylates MEF2A at the position S408 (Flavell et al., 2006; Shalizi et al., 2006), leading to a genomic response that consequentially impacts cellular morphology indirectly via transcriptional control of regulators of the cytoskeleton. Such regulators have recently been identified and linked to OT signaling by the group of J. Bakos, who found increased expression of the actin binding proteins drebrin, the intermediate filament vimentin, or the scaffolding protein SHANK3, under the influence of OT. This caused neurite outgrowth in human SH-SY5Y neuroblastoma or U-87MG glioblastoma cells (Bakos et al., 2018; Lestanova et al., 2016; Zatkova et al., 2018). As a consequence of neurite outgrowth, altered connectivity is observable due to increased synapse formation, which is under the OT-induced control of synaptic adhesion molecules like neuroligin 3 or neurexin 2 (Zatkova et al., 2019). Since OT is produced in the hypothalamus and we have found profound anxiolytic and anti-stress effects of OT infused into the hypothalamic paraventricular nucleus (Blume et al., 2008; Jurek et al., 2015; Jurek et al., 2012; Martinetz et al., 2019), we aimed to determine the intracellular effects of OT in a hypothalamic cell line, as opposed to neuroblastoma or glioblastoma cell types. As a cellular model of OTergic effects, we have characterized the rat hypothalamic neuronal cell line H32, which expresses MEF2A endogenously, and retract their neurites upon OT stimulation, caused by MEF2A activation (Meyer et al., 2018). Neurite retraction was blocked by siRNA-mediated knockdown of MEF2A, or pharmacological blockade of the OT receptor-induced MAPK pathway by U0126. This was seemingly in contrast to the above-mentioned studies showing OT-induced neurite outgrowth in SH-SY5Y or U-87MG cells, however, those are not hypothalamic neurons and might therefore react differently. In support of this hypothesis, we characterized the transcriptome of SH-SY5Y cells and found absent MEF2A expression. This phenotypical contrast led us to create a MEF2A knockout cell line, derived from our MEF2A-positive H32 cells (H32ΔMEF2A), using CRISPR-Cas9. In addition, we characterized another hypothalamic cell line (mHypoE-N11), which does not express endogenous MEF2A, and used those cells to overexpress MEF2A by plasmid transfection. By site-directed mutagenesis, we substituted the serine at position 408 to

aspartate, creating a permanent phospho-mimetic MEF2A mutant. This mutant, transfected into H32ΔMEF2A cells, served as control for phospho-site-specific effects of MEF2A, since MEF2A can be phosphorylated at three different residues, namely S408, Thr312, and Thr319, with opposing outcomes for gene transcription (Potthoff and Olson, 2007). Those three hypothalamic cell lines serve as internal controls in our experimental setup, and aid us to determine the morphological outcome of OT stimulation in hypothalamic cells in presence or absence of MEF2A. Cytoskeletal rearrangements are energy-consuming events requiring a proper functioning of the mitochondria. The organelles produce adenosine triphosphate (ATP) and provide energy for several cellular processes in neurons including action potential generation, but also morphological changes like neurite growth. Many neurodegenerative diseases with a loss of neuronal function and morphology show accompanying mitochondrial malfunctions (Mattson et al., 2008). Intriguingly, MEF2 regulates transcription of the mitochondrial NADH dehydrogenase 6 gene, which is essential for the function of the oxidative phosphorylation system (Naya et al., 2002; She et al., 2011), which ultimately regulates the production of ATP. In line with that, a significant proportion of ASD patients suffer from abnormal ATP production (Rossignol and Frye, 2014; Siddiqui et al., 2016), suggesting a central role for the OT-regulated transcription factor MEF2 in energy balance, structural plasticity, and ASD (also see (Brusco and Haas, 2015; Fiore et al., 2009; Meyer et al., 2018; Pfeiffer et al., 2010; Shalizi et al., 2006)). To test this hypothesis, we manipulated MEF2A activity in hypothalamic neurons and monitored morphological alterations and mitochondrial functionality.

2. Results

In order to study the impact of MEF2A in OT-induced effects on cellular morphology, we used cell lines that lacked, endogenously expressed, or were transfected with MEF2A.

The hypothalamic rat cell line H32 was subjected to CRISPR-Cas-mediated knockout of MEF2A (H32ΔMEF2A), and retransfected with either wild type rat MEF2A (H32ΔMEF2A^{MEF2A}) or the mutant version H32ΔMEF2A$^{MEF2A[S408D]}$, in which site-directed

mutagenesis at S408D mimicked a permanently phosphorylated, and therefore transcriptionally inactive transcription factor.

The mouse hypothalamic cell line mHypoE-N11 lacked MEF2A expression with levels below the detection limit of a qPCR. Transfection of those cells with a plasmid encoding for mouse MEF2A resulted in exogenous overexpression of MEF2A, as verified with immunofluorescence.

The cell lines created, and their MEF2A expression profile are summarized in Table 2.

Cell line	mHypoE-N11 (mouse)		H32 (rat)			
manipulation	wildtype	mHypoE-N11^{MEF2A}	wildtype	H32ΔMEF2A	H32ΔMEF2A^{MEF2A}	H32ΔMEF2A$^{MEF2A[S408D]}$ (inactive)
Level of MEF2A	-	++	+	-	++	++

Table 2. Summary of cell lines used and created in this study. MEF2A protein levels have been assessed by means of Western Blotting (Fig. A3). mHypoE-N11 derive from mouse hypothalamus neurons, and lack endogenous MEF2A expression. Plasmid transfection caused MEF2A overexpression in those cells (mHypoE-N11^{MEF2A}). H32 cells are immortalized neurons derived from a rat hypothalamus (Mugele et al., 1993) and show moderate endogenous expression of MEF2A (wildtype). CRISPR-Cas directed knock out of MEF2A produced H32ΔMEF2A cells, retransfection of intact MEF2A into H32ΔMEF2A cells rescued MEF2A expression (H32ΔMEF2A^{MEF2A}).

Treatment of mouse hypothalamic MEF2A-deficient mHypoE-N11 cells (see Tab. 2), with increasing concentrations (10, 100 and 250 nM) of OT overnight led to a dose-dependent increase in neurite length, which reached significance in the 100 and 250 nM treatment group, but not in the 10 nM group (Fig. 1A). Statistical analyses for all figures are summarized in Table 3, and we relegate the reader to the table for details on p values and effect sizes.

Overexpressing MEF2A in mHypoE-N11 cells by plasmid transfection with subsequent OT stimulation 48 h later, revealed a significant OT-induced retraction of neurites after 12 h in all doses tested (Fig. 1B). Successful overexpression of MEF2A was controlled by immuno-staining with an MEF2A-specific antibody (Fig. 1C). As expected, we found mainly nuclear location of MEF2A, with partial cytosolic location, representing a normal localization of the transcription factor (Potthoff and Olson, 2007).

Neither of the effects on neurite length was caused by altered cell viability. We found no decrease in cellular viability in H32 or H32ΔMEF2A cells, and no increased cell viability in mHypoE-N11 cells under the influence of OT (Fig. A2). This suggests that the OT-induced morphological effects are primarily alterations of the cytoskeleton, and not mere side-effects of an apoptotic or otherwise constricted cell.
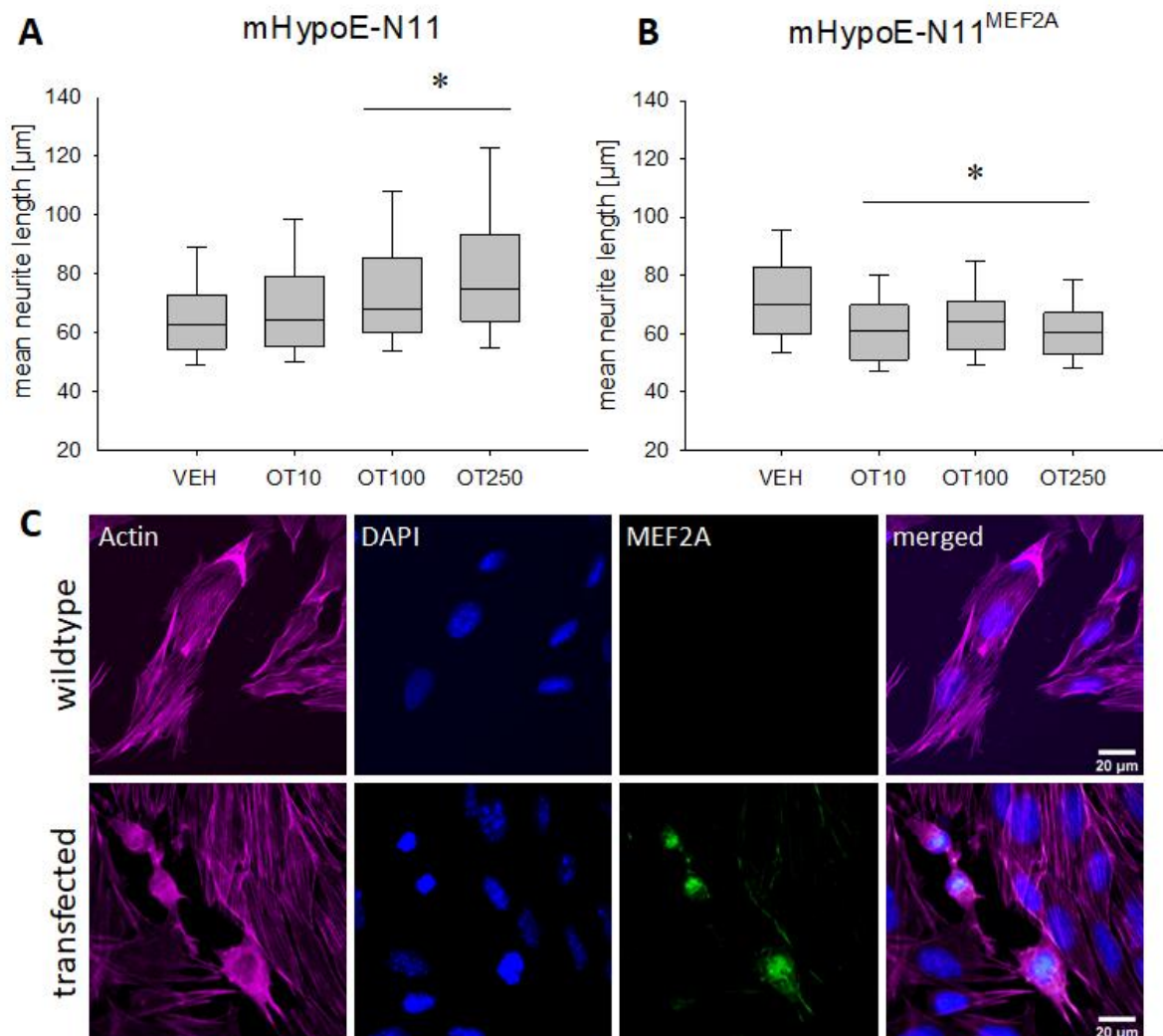

Figure 1. Effects of OT on neuronal morphology in the mouse hypothalamic cell line mHypoE-N11. (A) Median neurite length increases significantly in wildtype mHypoE-N11 cells treated overnight with 100 or 250 nM OT. * $p < 0.012$ vs VEH, n = 100 cells per treatment. (B) Treatment with 10, 100 and 250 nM of OT induces a significant neurite retraction in MEF2A overexpressing mHypoE-N11 cells. * $p < 0.003$ vs VEH, n = 100 cells per treatment. (C) Representative images of immunofluorescence labelling for MEF2A. Images were sequentially recorded for F-actin (Phalloidin, red, first column), chromatin (DAPI, blue, second column), and MEF2A (green, third column). Merged images are shown for each row in the fourth column. Labels left to the columns indicate the respective cell type (wildtype vs transfected).

Having established the 'gain-of-function-MEF2A' model with the mHypoE-N11 cells, we asked if a loss-of-MEF2A-function' model would reverse the OTergic effect on cellular

morphology. To obtain a permanent knockout of MEF2A, we made use of the CRISPR-Cas9 technology to create a monoclonal knockout cell line derived from a single edited H32 clone. The efficiency of the knockout was validated by western blot.

In contrast to OT-induced neurite retraction in H32 wildtype cells, we found neurite elongation after stimulating H32ΔMEF2A cells overnight with 100 and 250 nM OT (Fig. 2A). Retransfection of those knockout cells with an intact wildtype MEF2A reversed the effect and initiated OT-induced neurite retraction (Fig. 2B, light blue columns). However, when a phospho-mimetic, permanently inactive MEF2A [S408D] mutant was re-transfected, neurite elongation was observed (Fig. 2B, dark blue columns). This cellular response was comparable to the H32ΔMEF2A cells (Fig. 2A), revealing the S408 residue as the main phosphorylation site that orchestrates the OT effect on cellular morphology.
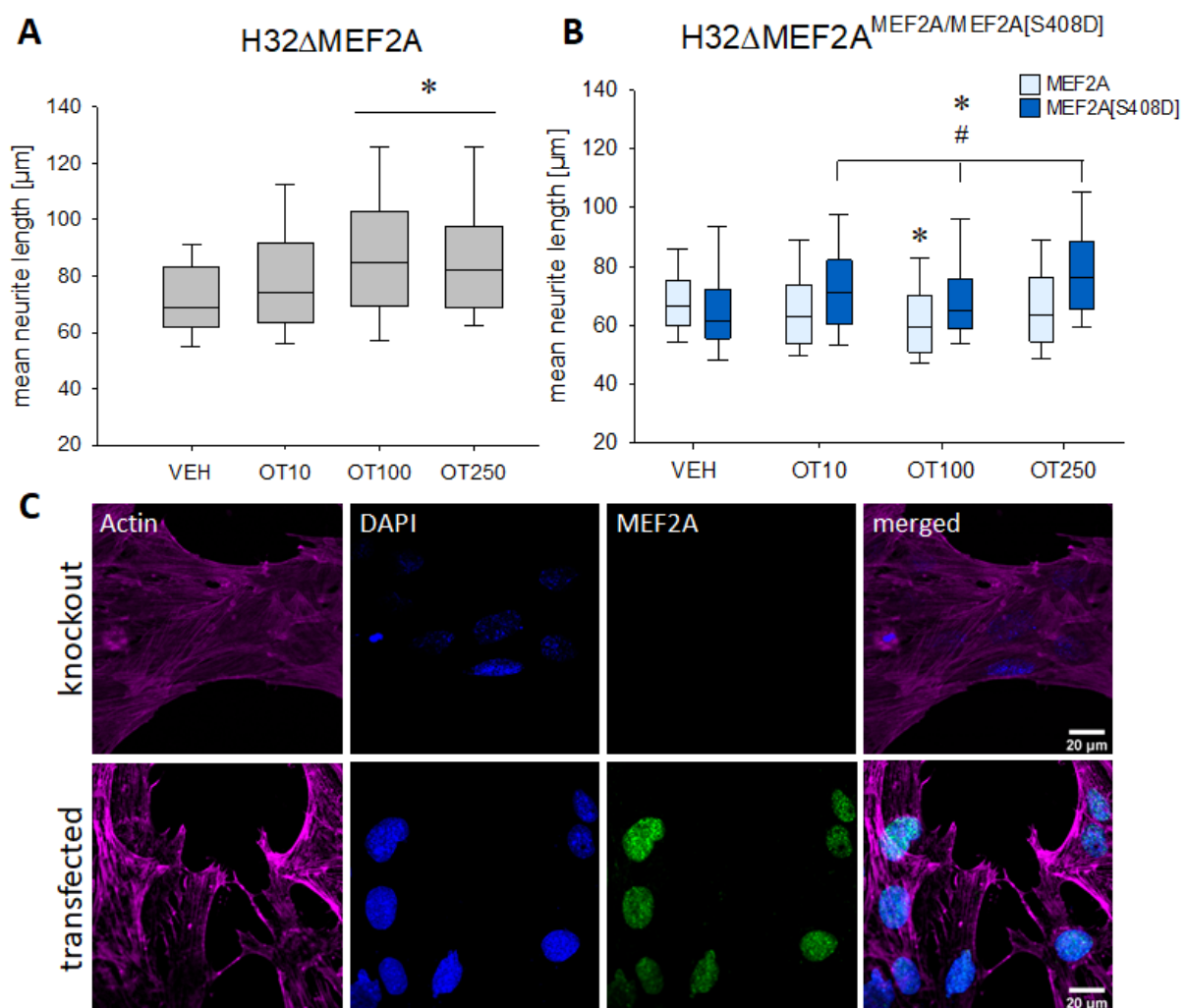

Figure 2. Effects of OT on neuronal morphology in the rat hypothalamic cell line H32. (A) Incubation of H32ΔMEF2A cells with 100 or 250 nM OT leads to a significant neurite elongation. * $p < 0.001$ vs VEH, n = 100 cells per treatment. (B) H32ΔMEF2A cells were retransfected with wildtype MEF2A and a mutant version

MEF2A[S408D], which mimics a permanently phosphorylated and therefore inactive MEF2A. The wildtype MEF2A generated OT-induced neurite retraction, whilst the mutant MEF2A lacked the ability to induce neurite retraction. Instead, the mutants response to OT resembled the MEF2A knockout cells. $n = 100$ cells per treatment. Two-way-ANOVA, $*$ $p < 0.031$ treatments vs VEH within the same group, $\#$ $p < 0.002$ groups (wildtype vs mutant) within the same treatment. (C) Representative images of immunofluorescence labelling for MEF2A. Images were sequentially recorded for F-actin (Phalloidin, red, first column), chromatin (DAPI, blue, second column), and MEF2A (green, third column). Merged images are shown for each row in the fourth column. Labels left to the columns indicate the respective cell type (knockout vs transfected).

We have shown in a previous publication (Meyer et al., 2018) that incubation of H32 cells with 100 nM OT overnight led to a dephosphorylation, and therefore activation, of MEF2A at S408, compared to VEH treated cells. This effect is indirectly mediated via the MAPK pathway, as it is reversed to basal by the MEK1/2 inhibitor U0126.

In the present study, OT stimulation led to decreased MEF2A S408 phosphorylation (One-way ANOVA $p = 0.056$, independent t-test VEH vs OT $p = 0.006$), whereas addition of CaN-inhibitor reversed the phosphorylation back to basal (Fig. 3A).

To test whether the observed CaN-activation is anyhow related to the MAPK pathway, we assessed MEK1/2 phosphorylation after OT/CaN-inhibitor treatment. Our Western Blot analysis revealed a MAPK pathway activation after OT treatment irrespective of the CaN inhibitor application, indicated by persistent MEK1/2 phosphorylation in the presence or absence of the CaN-inhibitor. The inhibitor alone, despite a visual increase, had no significant effect on MEK1/2 phosphorylation (Fig. 3B). As expected, those effects translated into morphological changes, i.e. OT treatment (as shown in Fig. 2B and (Meyer et al., 2018)) reduced neurite length from about 100 µm to about 75 µm, an effect that was blocked by the CaN inhibitor (Fig. 3C). In line with this data, when CaN was blocked in mHypoE-N11 cells (which don't express MEF2A), OT retained its ability to increase neurite length (Fig. 3D). This is in line with our hypothesis of the central role for the CaN-MEF2A pathway in OT-induced neurite retraction, but when MEF2A is absent, OT induces neurite outgrowth.
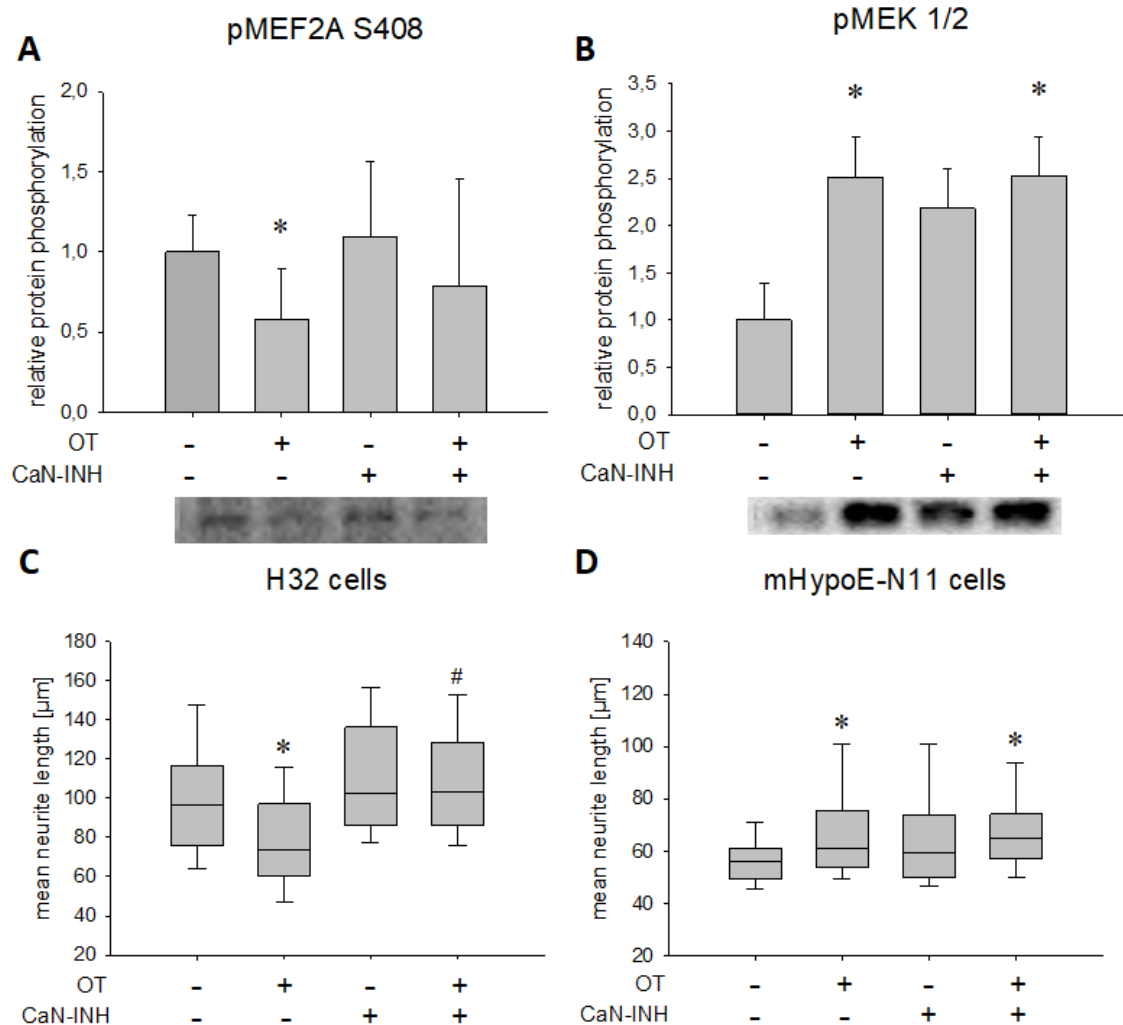
Figure 3. Effect of OT stimulation and calcineurin inhibition on phosphorylation of S408 of MEF2A and MEK1/2 as well as on the median neurite length in H32 cells. (A) Relative MEF2A S408 phosphorylation analyzed by Western Blot in whole cell lysate after treatment with VEH, OT, in presence or absence of a CaN inhibitor (CaN-INH), with representative Blot below. Overnight incubation of wildtype H32 cells with 100 nM OT led to a significant dephosphorylation of MEF2A at S408 compared to VEH treated cells. This effect is dependent on CaN activity as it is reversed to basal by a CaN-INH. The inhibitor without OT had no effect on MEF2A phosphorylation (n = 6). (B) Relative phosphorylation of MEK1/2 analyzed by Western Blot in whole cell lysate after treatment with VEH, OT, in presence or absence of a CaN inhibitor, with representative Blot picture below. Treatment of the cells with 100 nM OT overnight led to a significant phosphorylation of MEK1/2 compared to VEH. Statistical analysis using One-way ANOVA revealed no significant effect of the inhibitor treated cells, but a significant phosphorylation of MEK1/2 when cells were treated with OT and the CaN-INH. (C) In H32 cells, 100 nM of OT led to a significant retraction compared to VEH while inhibition of CaN results in an elongation of neurites overnight compared to VEH and OT. Combining the OT treatment with a CaN-INH increased the neurite length significantly. n = 100 per treatment, * p < 0.001 vs VEH-treated cells, # p < 0.001 vs OT-treated cells. (D) Incubation of mHypoE-N11 cells with 100 nM OT overnight led to an increased neurite length. Inhibition of CaN had no effect on the neuronal morphology, in line with the absent MEF2A expression in this cell line. n = 50 per treatment, * p < 0.05 vs VEH-treated cells.

For examination of mitochondrial function, we analyzed intact H32 wildtype and H32ΔMEF2A cells with the Agilent Seahorse XF Cell Mito Stress Test Kit. After application of different stressors to the cells, oxygen consumption rate is measured, which serves as indicator for mitochondrial functioning (Fig. 4A). H32ΔMEF2A cells showed a significantly higher maximal respiration (Fig. 4B) as well as spare respiratory capacity (Fig. 4C) compared to the MEF2A expressing H32 wildtype cells. This increased respiratory capacity in the H32ΔMEF2A cells suggests an inhibitory role for MEF2A in mitochondrial functioning. As direct consequence of this altered mitochondrial performance, basal cellular ATP content was significantly elevated in the H32ΔMEF2A cells, when compared with the wildtype cells (Fig. 4D). This additional energy supply might contribute to the cytoskeletal rearrangements that cause neurite elongation observed under OT treatment.

Neurite outgrowth serves to increase cell-cell contacts, which we hypothesized to simultaneously decrease cell-matrix contacts (Bikbaev et al., 2015; Chklovskii, 2004). As representative indicator for decreased cell-matrix contacts, we assessed integrin ß1 receptor expression (Tomaselli et al., 1993), and found decreased protein expression in H32ΔMEF2A cells compared to H32 wildtype cells (Fig. 4E).
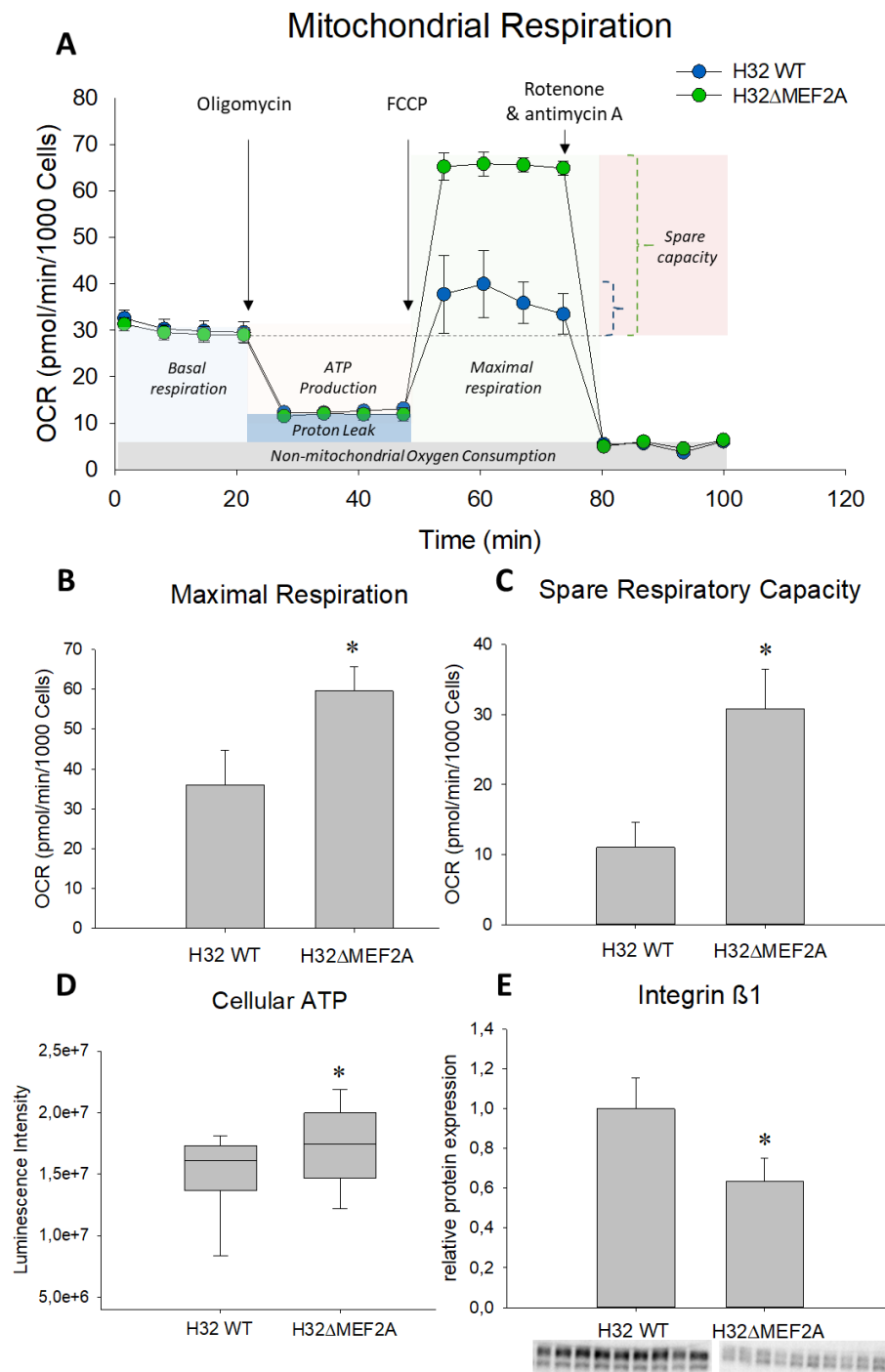
Figure 4. Effect of MEF2A knockout on mitochondrial function and neuronal connectivity. (A) Agilent Seahorse XF Cell Mito Stress Test profile shows oxygen consumption rate (OCR) in in H32 wildtype (WT) and H32ΔMEF2A cells representing key parameters of mitochondrial function. (B) and (C) OCR of both cell lines in the mitochondria stress test measured by Seahorse. H32ΔMEF2A cells show a significantly increased maximal respiration (* p = 0.004) and spare respiratory capacity (maximal vs basal respiration, * p = 0.01) compared to H32 cells. n = 3 test repetitions with 4 measurement replicates per group. (D) Cellular ATP content under basal conditions is significantly higher in H32ΔMEF2A than H32 WT cells. n = 24 per group; * p = 0.038. (E) Relative protein expression of Integrin ß1 is significantly downregulated in H32ΔMEF2A cells compared to H32 WT cells. n (H32 WT) = 9, n (H32ΔMEF2A) = 10; * p < 0.001.

3. Discussion

In recent publications, OT has been considered as a potential treatment for the alleviation of adverse psychiatric traits, e.g. ASD-related symptoms (Hurlemann, 2017; Kosfeld et al., 2005; Meyer-Lindenberg et al., 2011; Tost et al., 2010). The effects range from improving social skills in autistic children (Parker et al., 2017; Yatawara et al., 2015) to increased reciprocal trust in adult healthy probands (Kosfeld et al., 2005). However, the underlying molecular mechanism of the OT's alleviating properties on the symptoms of ASD are not fully understood. Considering the cellular changes apparent in ASD patients, we focused on the main parameters of cellular morphology, mitochondrial function and neuronal connectivity in this study, providing evidence for MEF2A as central regulator of those processes (Fig. 5).
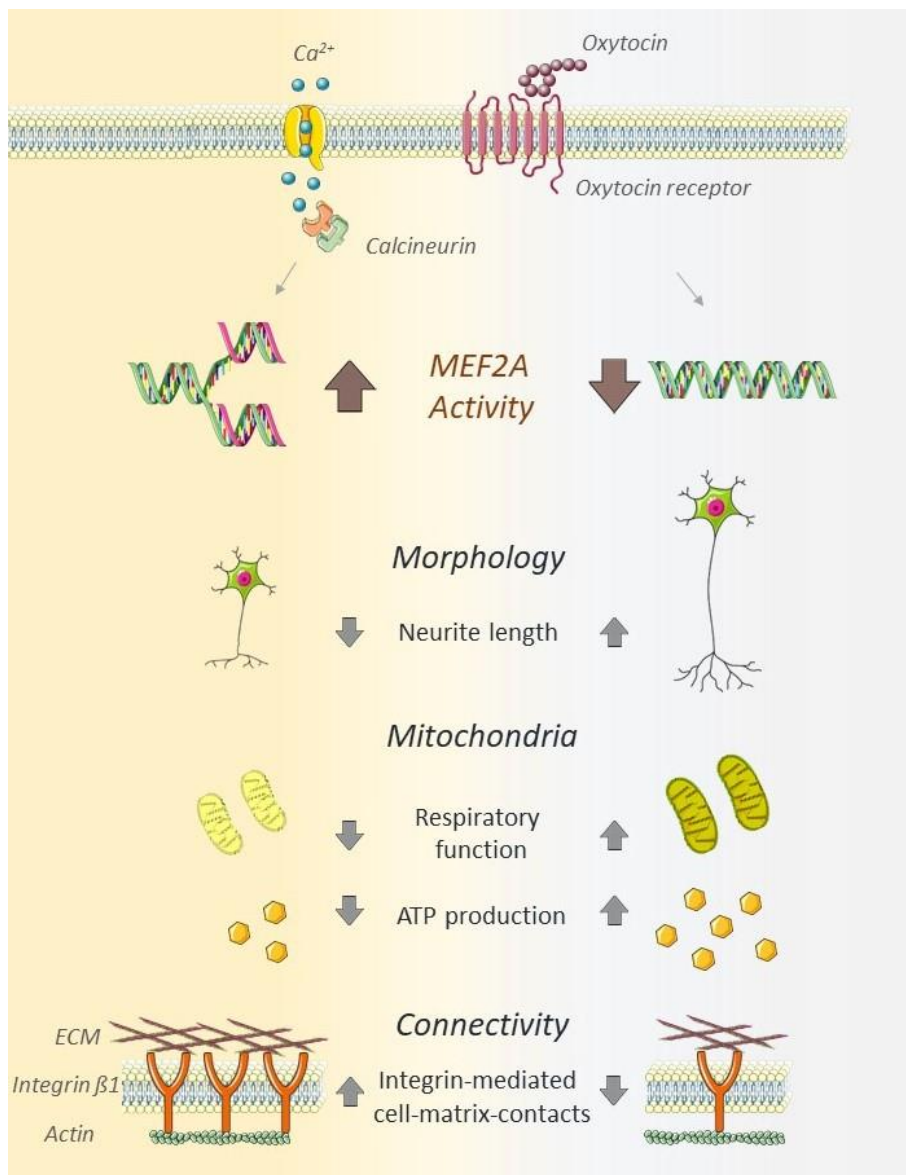
Figure 5. Schematic summary of MEF2A activity in OT-stimulated neurons. Neuronal MEF2A activity, induced by OT, reduces neurite length, decreases mitochondrial respiratory function, decreases ATP production, and increases ß-integrin-mediated cell-matrix contacts. Absence or inhibition of MEF2A induces neurite outgrowth, increased respiratory function, ATP production, and decreased cell-matrix connectivity. The schematic art pieces used in this figure were provided by Servier Medical art (http://servier.com/Powerpoint-image-bank). Servier Medical Art by Servier is licensed under a Creative Commons Attribution 3.0 Unported License.

We have identified the transcription factor MEF2A as the defining parameter that shifts the OT-induced neuronal response from neurite outgrowth towards neurite retraction. Knockin or knockout of MEF2A produced dichotomic effects on neuronal morphology, but only in

the presence of OT. When MEF2A is expressed, OT leads to a transcriptional activation by a dephosphorylation of the inhibitory site S408 of MEF2A, which promotes a switch from sumoylation to acetylation at Lys403 (Shalizi et al., 2006) and subsequent inhibition of dendritic morphogenesis (Shalizi et al., 2007). In contrast, when we transfected MEF2A knockout cells with the transcriptionally inactive mutant (H32ΔMEF2A$^{MEF2A[S408D]}$), sumoylation at Lys403 is retained and dendritic morphogenesis can occur. Interestingly, the knockout of MEF2A and its phospho-mimetic mutation did not just inhibit neurite retraction, but actively induced neurite outgrowth under the influence of OT. This implies alternative OTR-coupled pathways, which are silenced or overruled when MEF2A is expressed and active. One potential pathway is the MAPK pathway, which is activated by the OTR, but not affected by the MEF2A knockout or inhibition of CaN. The MAPK pathway has been associated with OT-induced anxiolysis, i.e. reduction of anxiety-like behavior in rats (Blume et al., 2008; Jurek et al., 2015; Jurek et al., 2012; Martinetz et al., 2019; van den Burg et al., 2015) and targets transcription factors like CREB and its cofactor CRTC3 (Jurek et al., 2015; Tomizawa et al., 2003). The MAPK pathway is certainly one of the main effectors of OTR signaling (Jurek and Neumann, 2018); however, it might not be directly linked to MEF2A activation, mainly because the S408 residue requires dephosphorylation, not phosphorylation, for full transcriptional activation. Evidence from hippocampal neurons suggests that a calcium-dependent activation of MEF2A requires the CaN-dependent dephosphorylation of MEF2A (Flavell et al., 2006; Shalizi et al., 2006). Based on this data, we identified CaN as the central part of a signaling cascade coupled to the OTR and thereby influencing the morphological response. Inhibiting CaN diminished the OT-induced neurite retraction in the H32 cells, strongly suggesting CaN as the upstream phosphatase responsible for OT-induced MEF2A activation. Moreover, mHypoE-N11 cells that lack MEF2A as a target of CaN, should not be affected by CaN inhibition. Indeed, blocking CaN activity did not interfere with OT-induced (MEF2A-independent) neurite elongation. Since the actions of CaN and MAPK signaling pathways have been shown to be co-dependent (Ichida and Finkel, 2001; Molkentin, 2004; Zhou et al., 2001), we tested MEK1/2 activity under OT / CaN-inhibition conditions. In line with our hypothesis, OT-induced MEK1/2 phosphorylation was not

affected by CaN inhibition, implying a direct activation of CaN by OTR-mediated Ca^{2+}-influx through either TrpV2 channels (van den Burg et al., 2015), or release from intracellular stores ((Jurek and Neumann, 2018) and references therein).

Furthermore, we provide evidence that a knockout of MEF2A has fundamental effects on mitochondrial functioning. While the basal respiration remains unaffected, the induced maximal respiration and spare respiratory capacity is significantly disinhibited compared to the wildtype cells. Next, we asked whether the increased respiratory capacity correlates with the ATP levels available for the cells. Interestingly, we found a significantly higher cellular ATP content under basal conditions in the H32ΔMEF2A cells. Although basal respiration does not differ between the two cell types, the increased respiratory capacity of the H32ΔMEF2A cells allows them to produce more ATP on-demand, mainly due to the use of the more efficient aerobic pathway (see Energy Map Fig. A1). The elevated ATP level present in the H32ΔMEF2A cells might be pivotal for the OT-induced neurite outgrowth. Changes in neurite outgrowth and plasticity are strongly intertwined processes implicated in the regulation of neuronal connectivity. Recent findings indicate that a state of neuronal hyperconnectivity may play an essential role in the etiology of ASD (Tang et al., 2014; Zaslavsky et al., 2019; Zhang et al., 2016). Many genes which have been associated with ASD and changes in neuronal connectivity belong to the integrin family (Lilja and Ivaska, 2018) and Ingenuity Pathway Analysis in myotube cells with MEF2 downregulations revealed that integrin signaling is one of the few pathways targeted by all MEF2 isoforms (Estrella et al., 2015). One member of this family is integrin ß1, a cell surface receptor linking the actin cytoskeleton with the extracellular matrix (ECM), mediating cell adhesion and thereby information that influences cellular morphology (Werner and Werb, 2002). We could show that this receptor is significantly downregulated in the H32ΔMEF2A cells. The effects of the MEF2A knockout on the mitochondrial function and the integrin signaling might not be causally connected. However, it has been suggested that alterations in mitochondrial function and integrin-mediated cell adhesion are functionally coupled processes (Werner and Werb, 2002). A crosstalk between cell adhesion and mitochondria is feasible, since it has

been shown that mitochondria react to ECM composition changes, and in turn, modifications of the ECM can result as a consequence of mitochondrial functioning (de Cavanagh et al., 2009). Mitochondria play a role in the mechanosensing processes of cells since mechanical forces from the ECM are transmitted to the mitochondria via focal adhesions (Bartolak-Suki et al., 2017). Therefore, it might be possible that the MEF2A knockout directly affects the mitochondria by targeting the mitochondrial transcriptome or indirectly via mechanobiological changes transmitted by integrin receptors into the cells.

Taken together, our results reveal a central role for MEF2A in the OT-induced regulation of neuronal morphology, connectivity, as well as mitochondrial function.

4. Materials and Methods

Cell culture

Rat hypothalamic H32 cells (kindly provided by Prof. Greti Aguilera (NICHD, Bethesda, MD)) and mouse hypothalamic mHypoE-N11 cells (kindly provided by Prof. Eugen Kerkhoff, University of Regensburg), were cultured in DMEM (#D8437, Sigma Aldrich), supplemented with 10% heat inactivated Gold fetal bovine serum (#FBS-HI-11A, Capricorn, Germany), and Penicillin/Streptomycin (#P4333, Sigma Aldrich) at 37 °C and 5% CO_2 until 80% confluency. Passaging was performed at least once a week by gentle trypsinization. Cells were counted and seeded at $3x10^6$ cells/75cm² density. Cell counts were recorded and compared between wildtype and knockout cell lines to extrapolate proliferation rates.

CRISPR-cas9 mediated knock out of MEF2A

The rat hypothalamic neuronal cell line H32 served as host to create an MEF2A knockout cell line (H32ΔMEF2A), using the Alt-R® CRISPR-Cas9 system (IDT, Coralville, USA). RNP complexes were composed of the functional gRNA duplex, containing the sequence-specific crRNA (sequence ID: Rn.Cas9.MEF2A.1.AC; 5'-A*C*A*G*A*C*C*T*C*A*C*G*G*T*A*C*C*A*A*A-3') and the ATTO 550-labeled tracrRNA in nuclease-free duplex buffer, and the S. p. Cas9 Nuclease 3NLS. The complexes

were transfected by cationic lipid delivery using Lipofectamine™ RNAiMAX Transfection Reagent (Invitrogen, Carlsbad, USA) and Opti-MEM (Gibco). Transfected single-cells were obtained 2 h after transfection by cell sorting and re-cultured for several weeks. The genotype was assessed by means of western blot.

Transfection of H32 and mHypoE-N11 cells with MEF2A overexpression plasmids

For morphological analyses, cells were transfected with plasmids (VectorBuilder) by electroporation using the manufacturer's Nucleofector (Thermo Scientific) protocol. 1 million cells were transfected with 0.5 µg of rat/mouse MEF2A plasmids. After 48 h incubation time, cells were further processed. The mouse hypothalamic cell line mHypoE-N11 was transfected with wildtype mouse MEF2A, resulting in mHypoE-N11^{MEF2A} cells. H32ΔMEF2A cells were transfected with either the wildtype variant of MEF2A (H32ΔMEF2A^{MEF2A}) or a phospho-mimetic MEF2A mutant (H32ΔMEF2A$^{MEF2A[S408D]}$).

Cell stimulations

Cells were stimulated overnight with 10, 100 or 250 nM of OT (Bachem, Germany) in cell culture dishes or chamber slides (BD Falcon, Germany). For the inhibition of CaN, CaN autoinhibitory peptide (#1891, Tocris) was used at a concentration of 10 µM (Perrino et al., 1995). Cells were pretreated with the inhibitor for 30 min and stimulated with the according treatment.

Protein isolation

For the extraction of proteins from OT- or vehicle stimulated 80% confluent H32 cells, stimulation medium was removed and cells were washed with 5 ml ice-cold PBS (#D8537, Sigma Aldrich). Cells were scraped in 1 ml ice-cold PBS using a cell scraper (#83.1830, Sarstedt), collected in 15 ml tubes in PBS, centrifuged at 300g, 4 °C for 5 min, and the resulting cell pellet was resuspended in 30-100 µl RIPA lysis buffer (R0278, Sigma Aldrich)

supplemented with HALT Inhibitor and EDTA (78444, Thermo Fisher) to obtain whole cell lysates.

Western Blot

Western Blot analysis was conducted as previously described in Meyer at al. 2018. Briefly, 15 or 40 µg of whole cell extract were loaded and separated in a 12% Mini PROTEAN or Criterion TGX Stainfree gel (Bio-Rad), respectively. Semi-dry blotting of separated proteins to nitrocellulose membranes was conducted using the FAST-Blotter by Bio-Rad. Uniform total protein loading was controlled for by the Stainfree total protein method by Bio-Rad. Specific antibodies for MEF2A, pMEFA S408, pMEK 1/2 and Integrin ß1 (Tab. 1) indicated activity and expression levels of the protein of interest.

Antibody	Company and Cat number	Dilution and diluent	Secondary antibody
MEF2A total	Acris AP06372PU-N	1:2000 in 5% MP	HRP-coupled anti-rabbit
pMEF2A S408	CusAb PA000728	1:5000 in 5% BSA	HRP-coupled anti-rabbit
pMEK1/2 4199	Cell Signaling 9154	1:5000 in 5% BSA	HRP-coupled anti-rabbit
Integrin ß1 (N-20)	Santa Cruz sc-6622	1:1000 in 5% BSA	HRP-coupled anti-goat

Table 1. Summary of antibodies used in this study with according dilution and host.

Immunofluorescence

mHypoE-N11 cells and mHypoE-N11[MEF2A], as well as H32ΔMEF2A and H32ΔMEF2A[MEF2A] cell lines were seeded on Chamber slides (BD-Falcon, #08-774-25) at 6×10^4 cells per chamber and cultured overnight in growth medium at 37 °C / 5% CO_2. Next, the growth medium was removed and cells were briefly rinsed with warm PBS. The PBS was removed and replaced with 500 µl ice-cold 3% Glyoxal-solution (+20% EtOH, Acetic acid,

pH= 4-5) for 20 min. After washing the cells twice with PBS-T (0,5% tween), unspecific binding sites were blocked (PBS+0,5% TritonX, 1% Glycine, 10% BSA, 1% Normal goat serum) for 30 min, and antibody incubated overnight at according dilution. After intense washing with PBS-T, secondary antibody (BioTrend, CF488A highly cross-adsorbed #20123) were incubated at 1:500 in PBS for 30 min. After washing, cells were incubated with Phalloidin-iFluor 594 Reagent (abcam ab176757), mounted with ProLong Glass-Antifade mounting medium with DAPI (Thermo Scientific, #P36982) and covered by cover slips (Thor Labs, refraction index 1,5; #CG15KH). Images were taken on a Zeiss AiryDisc Confocal microscope with a 63x objective with identical laser and gain intensities to guarantee comparability between images.

Morphological characterization

For nucleus staining, Hoechst 33342 stain (Thermo Scientific, H1399) was added to the stimulation medium in the 6 well plates where cells were stimulated, and incubated for 30 min at 37 °C. The cells grown in cell culture dishes were washed with 1 ml PBS and subsequently fixed by gently adding 3% Glyoxal solution for 20 min (3% glyoxal in H2O, #128465, Sigma Aldrich, supplemented with 20% EtOH and acetic acid to acquire pH = 5). All Pictures were taken using the ZOE Fluorescence microscope (Bio-Rad). Neurite outgrowth was determined by manually tracing the length of the longest neurite per cell (using ImageJ Fiji software) for all cells in a field that had an identifiable neurite and for which the entire neurite arbor could be visualized. Length of the neurite was measured from the edge of nucleus to the apical end of the projection. Only those neurites were evaluated that did not contact other cells. At least two members of the team independently evaluated the neurite length in a blinded manner.

Cell viability assay

Cellular viability was tested using the PrestoBlue Cell Viability Assay (A13261, Invitrogen) according to the manufacturer's protocol and as described in (Meyer et al., 2018). Briefly, 10×10^3 cells per well were seeded the day before the test in a 96-well-plate in growth

medium. The volume of the treatment and medium for the stimulation was calculated to a total of 90 µl per well. 10 µl of PrestoBlue Reagent were added directly to the cells, incubated for 30 min before reading the fluorescence intensity with a FluoStar Plate reader (BMG).

Mitochondrial respiration analysis

The oxygen consumption rate (OCR) of intact H32 and H32ΔMEF2A cells was measured with the Agilent Seahorse XF Cell Mito Stress Test Kit (Agilent Technologies, Waldbronn, Germany) according to manufacturer's protocol. The live cell assay monitors OCR in real time and assesses the key parameters of mitochondrial function. The mitochondrial stress compounds used for this assay are Oligomycin (1 µM), Carbonyl cyanide-4 (trifluoromethoxy) phenylhydrazone (FCCP; 2 µM), Rotenone/Antimycin A (1 µM). On the day before the measurement, 20×10^3 cells were seeded in matrigel coated XFp 8-well miniplates (Agilent Technologies, Waldbronn, Germany) at 37 °C, humidified air and 5% CO_2. Cartridges were prepared according to the provided protocol. The obtained values were normalized to the cell number present in the region of interest reflecting the field of measurement by ImageJ. Data was analyzed using the WAVE software (Agilent Technologies, CA, USA) according to manufacturer's instructions.

CellTiter-Glo 2.0 assay

The CellTiter-Glo 2.0 assay (Promega) was conducted to measure cellular ATP content under basal/non-stimulated conditions in H32 and H32ΔMEF2A cells, according to the manufacturer's protocol. Briefly, 10×10^3 cells per well were seeded the day before in a Nunclon Delta Surface 96-well plate (Thermo Scientific, #136101). On the next day, an ATP standard curve was generated and an equal volume of Cell Titer Reagent 2.0 added to the culture medium present in each well. After 12 min incubation, luminescence intensity was recorded with the GloMax Luminometer (Promega). The assay was repeated three times.

Statistical analysis

Statistical analyses were performed using Sigma Plot (version 13.0, Systat Software). Parametric data was analyzed by t-test or one-way analysis of variance (ANOVA) followed by Holm-Sidak post hoc test. Non-parametric data was analyzed by the Mann-Whitney Rank Sum Test or Kruskal-Wallis ANOVA on ranks and the Tukey post hoc test. Statistical significance was accepted at $p < 0.05$. In morphological experiments, n represents number of cells, in Western Blots, n represents number of cell lysates, in the ATP and cell viability assays, n is number of wells. Parametric data are presented as mean + standard deviation (SD). Non-parametric data is represented in box plots as minimum, first quartile, median, third quartile, and maximum. Details on statistics have been summarized in Table 3.
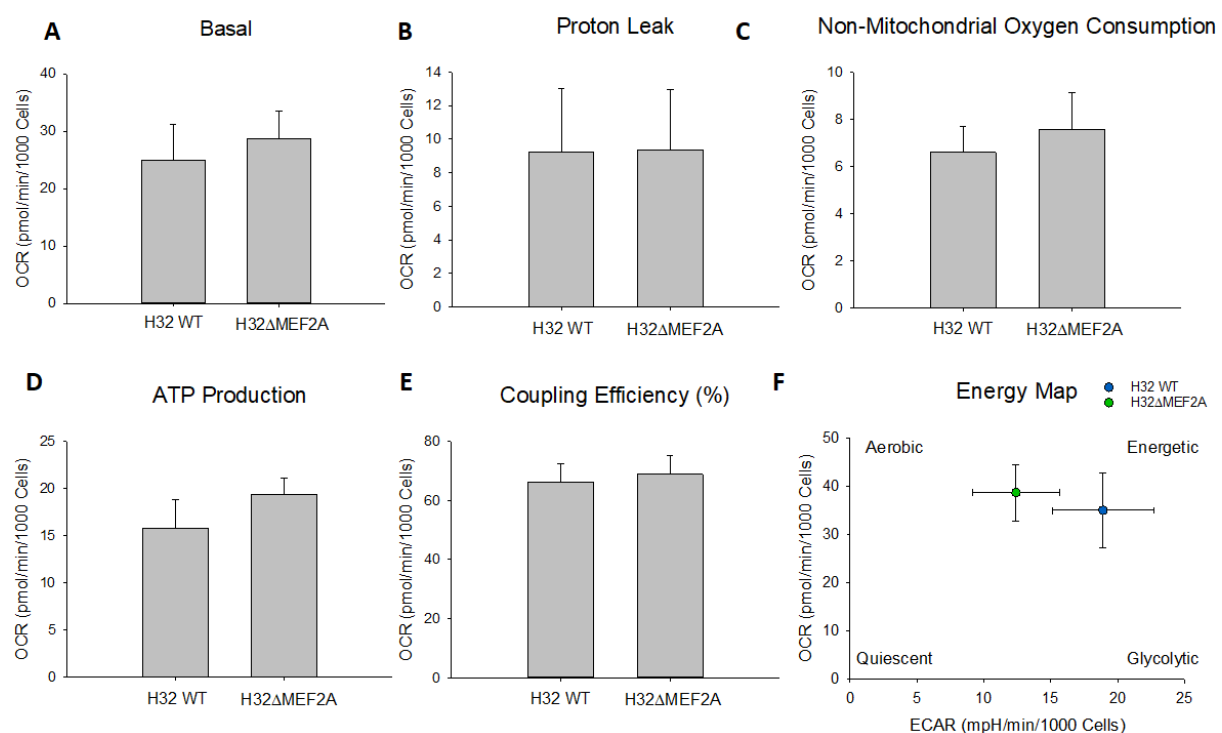
Appendix

Figure A1. Mitochondrial function in H32 wildtype and H32ΔMEF2A cells. n = 3 per group.
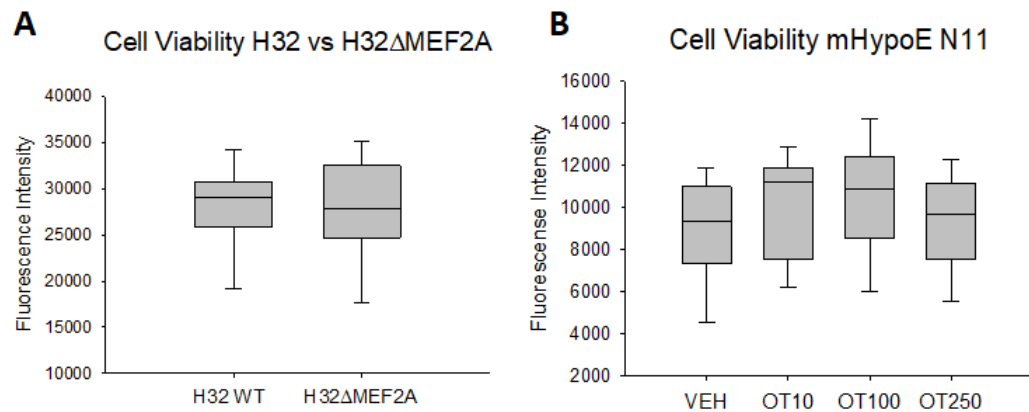
Figure A2. (A) Cell viability in H32 vs H32ΔMEF2A n = 24 per group. (B) Cell viability in OT-treated mHypoE-N11 cells. n = 22-24 per group.
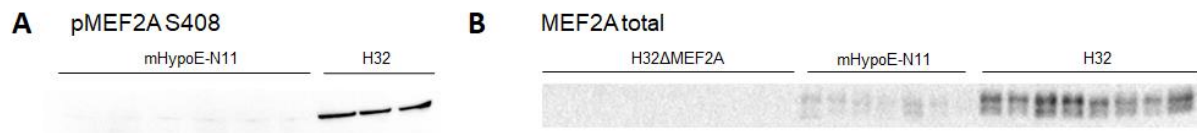

Figure A3. (A) and (B) Characterization of pMEF2A S408 and MEF2A total in mHypoE-N11, H32ΔMEF2A and H32 cells.

Conflicts of Interest: The authors declare no conflict of interest.

Abbreviations

MEF2A	Myocyte enhancer factor 2A
OT	Oxytocin
CaN	Calcineurin
MAPK	Mitogen activated protein kinase

References

Alaerts, K., Bernaerts, S., Vanaudenaerde, B., Daniels, N., and Wenderoth, N. (2019). Amygdala-Hippocampal Connectivity Is Associated With Endogenous Levels of Oxytocin and Can Be Altered by Exogenously Administered Oxytocin in Adults With Autism. Biological psychiatry Cognitive neuroscience and neuroimaging *4*, 655-663.

Bakos, J., Srancikova, A., Havranek, T., and Bacova, Z. (2018). Molecular Mechanisms of Oxytocin Signaling at the Synaptic Connection. Neural Plast *2018*, 4864107.

Bartolak-Suki, E., Imsirovic, J., Nishibori, Y., Krishnan, R., and Suki, B. (2017). Regulation of Mitochondrial Structure and Dynamics by the Cytoskeleton and Mechanical Factors. Int J Mol Sci *18*.

Bikbaev, A., Frischknecht, R., and Heine, M. (2015). Brain extracellular matrix retains connectivity in neuronal networks. Scientific reports *5*, 14527.

Blume, A., Bosch, O.J., Miklos, S., Torner, L., Wales, L., Waldherr, M., and Neumann, I.D. (2008). Oxytocin reduces anxiety via ERK1/2 activation: local effect within the rat hypothalamic paraventricular nucleus. The European journal of neuroscience *27*, 1947-1956.

Bringas, M.E., Carvajal-Flores, F.N., Lopez-Ramirez, T.A., Atzori, M., and Flores, G. (2013). Rearrangement of the dendritic morphology in limbic regions and altered exploratory behavior in a rat model of autism spectrum disorder. Neuroscience *241*, 170-187.

Brusco, J., and Haas, K. (2015). Interactions between mitochondria and the transcription factor myocyte enhancer factor 2 (MEF2) regulate neuronal structural and functional plasticity and metaplasticity. The Journal of physiology *593*, 3471-3481.

Carson, D.S., Berquist, S.W., Trujillo, T.H., Garner, J.P., Hannah, S.L., Hyde, S.A., Sumiyoshi, R.D., Jackson, L.P., Moss, J.K., Strehlow, M.C.*, et al.* (2015). Cerebrospinal fluid and plasma oxytocin concentrations are positively correlated and negatively predict anxiety in children. Molecular psychiatry *20*, 1085-1090.

Chklovskii, D.B. (2004). Synaptic connectivity and neuronal morphology: two sides of the same coin. Neuron *43*, 609-617.

de Cavanagh, E.M., Ferder, M., Inserra, F., and Ferder, L. (2009). Angiotensin II, mitochondria, cytoskeletal, and extracellular matrix connections: an integrating viewpoint. American journal of physiology Heart and circulatory physiology *296*, H550-558.

Descazeaud, V., Mestre, E., Marquet, P., and Essig, M. (2012). Calcineurin regulation of cytoskeleton organization: a new paradigm to analyse the effects of calcineurin inhibitors on the kidney. Journal of cellular and molecular medicine *16*, 218-227.

Estrella, N.L., Desjardins, C.A., Nocco, S.E., Clark, A.L., Maksimenko, Y., and Naya, F.J. (2015). MEF2 transcription factors regulate distinct gene programs in mammalian skeletal muscle differentiation. The Journal of biological chemistry *290*, 1256-1268.

Falougy, H.E., Filova, B., Ostatnikova, D., Bacova, Z., and Bakos, J. (2019). Neuronal morphology alterations in autism and possible role of oxytocin. Endocr Regul *53*, 46-54.

Fiore, R., Khudayberdiev, S., Christensen, M., Siegel, G., Flavell, S.W., Kim, T.K., Greenberg, M.E., and Schratt, G. (2009). Mef2-mediated transcription of the miR379-410 cluster regulates activity-dependent dendritogenesis by fine-tuning Pumilio2 protein levels. The EMBO journal *28*, 697-710.

Flavell, S.W., Cowan, C.W., Kim, T.K., Greer, P.L., Lin, Y., Paradis, S., Griffith, E.C., Hu, L.S., Chen, C., and Greenberg, M.E. (2006). Activity-dependent regulation of MEF2 transcription factors suppresses excitatory synapse number. Science (New York, NY *311*, 1008-1012.

Garcia-Cabezas, M.A., Barbas, H., and Zikopoulos, B. (2018). Parallel Development of Chromatin Patterns, Neuron Morphology, and Connections: Potential for Disruption in Autism. Frontiers in neuroanatomy *12*, 70.

Hurlemann, R. (2017). Oxytocin-Augmented Psychotherapy: Beware of Context. Neuropsychopharmacology *42*, 377.

Ichida, M., and Finkel, T. (2001). Ras regulates NFAT3 activity in cardiac myocytes. The Journal of biological chemistry *276*, 3524-3530.

Jurek, B., and Neumann, I.D. (2018). The Oxytocin Receptor: From Intracellular Signaling to Behavior. Physiological reviews *98*, 1805-1908.

Jurek, B., Slattery, D.A., Hiraoka, Y., Liu, Y., Nishimori, K., Aguilera, G., Neumann, I.D., and van den Burg, E.H. (2015). Oxytocin Regulates Stress-Induced Crf Gene Transcription through CREB-Regulated Transcription Coactivator 3. J Neurosci *35*, 12248-12260.

Jurek, B., Slattery, D.A., Maloumby, R., Hillerer, K., Koszinowski, S., Neumann, I.D., and van den Burg, E.H. (2012). Differential contribution of hypothalamic MAPK activity to anxiety-like behaviour in virgin and lactating rats. PloS one *7*, e37060.

Kosfeld, M., Heinrichs, M., Zak, P.J., Fischbacher, U., and Fehr, E. (2005). Oxytocin increases trust in humans. Nature *435*, 673-676.

Lautermilch, N.J., and Spitzer, N.C. (2000). Regulation of calcineurin by growth cone calcium waves controls neurite extension. J Neurosci *20*, 315-325.

Lestanova, Z., Bacova, Z., Kiss, A., Havranek, T., Strbak, V., and Bakos, J. (2016). Oxytocin Increases Neurite Length and Expression of Cytoskeletal Proteins Associated with Neuronal Growth. J Mol Neurosci *59*, 184-192.

Lilja, J., and Ivaska, J. (2018). Integrin activity in neuronal connectivity. Journal of cell science *131*, jcs212803.

Maes, M., Anderson, G., Betancort Medina, S.R., Seo, M., and Ojala, J.O. (2019). Integrating Autism Spectrum Disorder Pathophysiology: Mitochondria, Vitamin A, CD38, Oxytocin, Serotonin and Melatonergic Alterations in the Placenta and Gut. Curr Pharm Des *25*, 4405-4420.

Martinetz, S., Meinung, C.P., Jurek, B., von Schack, D., van den Burg, E.H., Slattery, D.A., and Neumann, I.D. (2019). De Novo Protein Synthesis Mediated by the Eukaryotic Elongation Factor 2 Is Required for the Anxiolytic Effect of Oxytocin. Biological psychiatry *85*, 802-811.

Mattson, M.P., Gleichmann, M., and Cheng, A. (2008). Mitochondria in neuroplasticity and neurological disorders. Neuron *60*, 748-766.

Meyer-Lindenberg, A., Domes, G., Kirsch, P., and Heinrichs, M. (2011). Oxytocin and vasopressin in the human brain: social neuropeptides for translational medicine. Nature reviews Neuroscience *12*, 524-538.

Meyer, M., Berger, I., Winter, J., and Jurek, B. (2018). Oxytocin alters the morphology of hypothalamic neurons via the transcription factor myocyte enhancer factor 2A (MEF-2A). Molecular and cellular endocrinology *477*, 156-162.

Molkentin, J.D. (2004). Calcineurin-NFAT signaling regulates the cardiac hypertrophic response in coordination with the MAPKs. Cardiovasc Res *63*, 467-475.

Morrow, E.M., Yoo, S.Y., Flavell, S.W., Kim, T.K., Lin, Y., Hill, R.S., Mukaddes, N.M., Balkhy, S., Gascon, G., Hashmi, A.*, et al.* (2008). Identifying autism loci and genes by tracing recent shared ancestry. Science (New York, NY *321*, 218-223.

Naya, F.J., Black, B.L., Wu, H., Bassel-Duby, R., Richardson, J.A., Hill, J.A., and Olson, E.N. (2002). Mitochondrial deficiency and cardiac sudden death in mice lacking the MEF2A transcription factor. Nature medicine *8*, 1303-1309.

Parker, K.J., Garner, J.P., Libove, R.A., Hyde, S.A., Hornbeak, K.B., Carson, D.S., Liao, C.P., Phillips, J.M., Hallmayer, J.F., and Hardan, A.Y. (2014). Plasma oxytocin concentrations and OXTR polymorphisms predict social impairments in children with and without autism spectrum disorder. Proceedings of the National Academy of Sciences of the United States of America *111*, 12258-12263.

Parker, K.J., Oztan, O., Libove, R.A., Sumiyoshi, R.D., Jackson, L.P., Karhson, D.S., Summers, J.E., Hinman, K.E., Motonaga, K.S., Phillips, J.M.*, et al.* (2017). Intranasal oxytocin treatment for social deficits and biomarkers of response in children with autism. Proceedings of the National Academy of Sciences of the United States of America *114*, 8119-8124.

Pfeiffer, B.E., Zang, T., Wilkerson, J.R., Taniguchi, M., Maksimova, M.A., Smith, L.N., Cowan, C.W., and Huber, K.M. (2010). Fragile X mental retardation protein is required for synapse elimination by the activity-dependent transcription factor MEF2. Neuron *66*, 191-197.

Pont, J.N., McArdle, C.A., and Lopez Bernal, A. (2012). Oxytocin-stimulated NFAT transcriptional activation in human myometrial cells. Molecular endocrinology (Baltimore, Md *26*, 1743-1756.

Potthoff, M.J., and Olson, E.N. (2007). MEF2: a central regulator of diverse developmental programs. Development (Cambridge, England) *134*, 4131-4140.

Rossignol, D.A., and Frye, R.E. (2014). Evidence linking oxidative stress, mitochondrial dysfunction, and inflammation in the brain of individuals with autism. Frontiers in physiology *5*, 150.

Sanborn, B.M. (2007). Hormonal signaling and signal pathway crosstalk in the control of myometrial calcium dynamics. Seminars in cell & developmental biology *18*, 305-314.

Shalizi, A., Bilimoria, P.M., Stegmuller, J., Gaudilliere, B., Yang, Y., Shuai, K., and Bonni, A. (2007). PIASx is a MEF2 SUMO E3 ligase that promotes postsynaptic dendritic morphogenesis. J Neurosci *27*, 10037-10046.

Shalizi, A., Gaudilliere, B., Yuan, Z., Stegmuller, J., Shirogane, T., Ge, Q., Tan, Y., Schulman, B., Harper, J.W., and Bonni, A. (2006). A calcium-regulated MEF2 sumoylation switch controls postsynaptic differentiation. Science (New York, NY *311*, 1012-1017.

She, H., Yang, Q., Shepherd, K., Smith, Y., Miller, G., Testa, C., and Mao, Z. (2011). Direct regulation of complex I by mitochondrial MEF2D is disrupted in a mouse model of Parkinson disease and in human patients. J Clin Invest *121*, 930-940.

Siddiqui, M.F., Elwell, C., and Johnson, M.H. (2016). Mitochondrial Dysfunction in Autism Spectrum Disorders. Autism Open Access *6*.

Tang, G., Gudsnuk, K., Kuo, S.H., Cotrina, M.L., Rosoklija, G., Sosunov, A., Sonders, M.S., Kanter, E., Castagna, C., Yamamoto, A.*, et al.* (2014). Loss of mTOR-dependent macroautophagy causes autistic-like synaptic pruning deficits. Neuron *83*, 1131-1143.

Tomaselli, K., Doherty, P., Emmett, C., Damsky, C., Walsh, F., and Reichardt, L. (1993). Expression of beta 1 integrins in sensory neurons of the dorsal root ganglion and their functions in neurite outgrowth on two laminin isoforms. The Journal of Neuroscience *13*, 4880-4888.

Tomizawa, K., Iga, N., Lu, Y.F., Moriwaki, A., Matsushita, M., Li, S.T., Miyamoto, O., Itano, T., and Matsui, H. (2003). Oxytocin improves long-lasting spatial memory during motherhood through MAP kinase cascade. Nature neuroscience *6*, 384-390.

Tost, H., Kolachana, B., Hakimi, S., Lemaitre, H., Verchinski, B.A., Mattay, V.S., Weinberger, D.R., and Meyer-Lindenberg, A. (2010). A common allele in the oxytocin receptor gene (OXTR) impacts

prosocial temperament and human hypothalamic-limbic structure and function. Proceedings of the National Academy of Sciences of the United States of America *107*, 13936-13941.

van den Burg, E.H., Stindl, J., Grund, T., Neumann, I.D., and Strauss, O. (2015). Oxytocin Stimulates Extracellular Ca2+ Influx Through TRPV2 Channels in Hypothalamic Neurons to Exert Its Anxiolytic Effects. Neuropsychopharmacology *40*, 2938-2947.

Werner, E., and Werb, Z. (2002). Integrins engage mitochondrial function for signal transduction by a mechanism dependent on Rho GTPases. The Journal of cell biology *158*, 357-368.

Xiong, T.Q., Chen, L.M., Tan, B.H., Guo, C.Y., Li, Y.N., Zhang, Y.F., Li, S.L., Zhao, H., and Li, Y.C. (2018). The effects of calcineurin inhibitor FK506 on actin cytoskeleton, neuronal survival and glial reactions after pilocarpine-induced status epilepticus in mice. Epilepsy Res *140*, 138-147.

Yatawara, C.J., Einfeld, S.L., Hickie, I.B., Davenport, T.A., and Guastella, A.J. (2015). The effect of oxytocin nasal spray on social interaction deficits observed in young children with autism: a randomized clinical crossover trial. Molecular psychiatry.

Ying, L., Becard, M., Lyell, D., Han, X., Shortliffe, L., Husted, C.I., Alvira, C.M., and Cornfield, D.N. (2015). The transient receptor potential vanilloid 4 channel modulates uterine tone during pregnancy. Science translational medicine *7*, 319ra204.

Young, A.M., Chakrabarti, B., Roberts, D., Lai, M.C., Suckling, J., and Baron-Cohen, S. (2016). From molecules to neural morphology: understanding neuroinflammation in autism spectrum condition. Molecular autism *7*, 9.

Yuen, K.W., Garner, J.P., Carson, D.S., Keller, J., Lembke, A., Hyde, S.A., Kenna, H.A., Tennakoon, L., Schatzberg, A.F., and Parker, K.J. (2014). Plasma oxytocin concentrations are lower in depressed vs. healthy control women and are independent of cortisol. Journal of psychiatric research *51*, 30-36.

Zaslavsky, K., Zhang, W.B., McCready, F.P., Rodrigues, D.C., Deneault, E., Loo, C., Zhao, M., Ross, P.J., El Hajjar, J., Romm, A*., et al.* (2019). SHANK2 mutations associated with autism spectrum disorder cause hyperconnectivity of human neurons. Nature neuroscience *22*, 556-564.

Zatkova, M., Bacova, Z., Puerta, F., Lestanova, Z., Alanazi, M., Kiss, A., Reichova, A., Castejon, A.M., Ostatnikova, D., and Bakos, J. (2018). Projection length stimulated by oxytocin is modulated by the inhibition of calcium signaling in U-87MG cells. J Neural Transm (Vienna) *125*, 1847-1856.

Zatkova, M., Reichova, A., Bacova, Z., and Bakos, J. (2019). Activation of the Oxytocin Receptor Modulates the Expression of Synaptic Adhesion Molecules in a Cell-Specific Manner. J Mol Neurosci *68*, 171-180.

Zhang, Z., Cao, M., Chang, C.W., Wang, C., Shi, X., Zhan, X., Birnbaum, S.G., Bezprozvanny, I., Huber, K.M., and Wu, J.I. (2016). Autism-Associated Chromatin Regulator Brg1/SmarcA4 Is Required for Synapse Development and Myocyte Enhancer Factor 2-Mediated Synapse Remodeling. Molecular and cellular biology *36*, 70-83.

Zhou, C.J., Yada, T., Kohno, D., Kikuyama, S., Suzuki, R., Mizushima, H., and Shioda, S. (2001). PACAP activates PKA, PKC and Ca(2+) signaling cascades in rat neuroepithelial cells. Peptides *22*, 1111-1117.